Detection of boson peak and fractal dynamics of disordered systems using terahertz spectroscopy

Tatsuya Mori [1,*], Yue Jiang,[1] Yasuhiro Fujii [2], Suguru Kitani,[3] Hideyuki Mizuno [4], Akitoshi Koreeda,[2] Leona Motoji,[1]
Hiroko Tokoro [1], Kentaro Shiraki,[1] Yohei Yamamoto [1], and Seiji Kojima [1]

[1]*Division of Materials Science, University of Tsukuba, 1-1-1 Tennodai, Tsukuba, Ibaraki 305-8573, Japan*
[2]*Department of Physical Sciences, Ritsumeikan University, 1-1-1 Noji-higashi, Kusatsu, Shiga 525-8577, Japan*
[3]*Laboratory for Materials and Structures, Tokyo Institute of Technology, 4259 Nagatsuta-cho, Midori-ku, Yokohama 226-8503, Japan*
[4]*Graduate School of Arts and Sciences, The University of Tokyo, Tokyo 153-8902, Japan*

The boson peak is a largely unexplained excitation found universally in the terahertz vibrational spectra of disordered systems; the so-called fracton is a vibrational excitation associated with the self-similar structure of monomers in polymeric glasses. We demonstrate that such excitations can be detected using terahertz spectroscopy. In the case of fractal structures, we determine the infrared light-vibration coupling coefficient for the fracton region and show that information concerning the fractal and fracton dimensions appears in the exponent of the absorption coefficient. Finally, using terahertz time-domain spectroscopy and low-frequency Raman scattering, we experimentally observe these universal excitations in a protein (lysozyme) system that has an intrinsically disordered and fractal structure and argue that the system should be considered a single supramolecule. These findings are applicable to amorphous and fractal objects in general and will be valuable for understanding universal dynamics of disordered systems via terahertz light.

I. INTRODUCTION

The Debye theory predicts the behavior of acoustic phonons in a D-dimensional crystalline system: The vibrational density of states [v-DOS, $g(\nu)$] should follow a power law, $g(\nu) \propto \nu^2$, where ν is frequency. In disordered materials, however, an anomaly appears in the acoustic phonon mode [1]. This so-called boson peak (BP) is a universal excitation in the terahertz (THz) region, where propagating sound waves end. The peak appears in the $g(\nu)/\nu^2$ spectrum of many amorphous solids. The origin of this deviation from the Debye model, while no doubt closely related to other low-temperature thermal phenomena observed universally in glassy materials [2,3], has long been an unresolved issue in glass physics.

There are other instances of universal dynamics in amorphous materials. For example, in a polymer glass system, the structure induced by the self-similar connectivity of structural units in the polymer chain has been shown to lead to fractal dynamics [4,5]. Fractal materials exhibit quasiparticle modes known as fractons, and have a non-Debye v-DOS $g(\nu) \propto \nu^{d_f - 1}$. Here d_f is the fracton dimension, which is independent of the Euclidean dimension D and also not identical to the fractal dimension of the material. Alexander and Orbach [4], the originators of the fracton concept, have conjectured that d_f always takes the value 4/3 in percolation clusters.

Interestingly, universal dynamics similar to those of disordered materials also appear in a few single crystals, which are obviously not disordered systems. BPs or other amorphous-like thermal behaviors have been observed in thermoelectric materials [6–9], pure relaxor materials [10], and atypical organic materials [11,12]. Theoretical studies [8,13–15] suggest that in these materials, off-center large-amplitude anharmonic vibration modes play a crucial role in the existence of universal glasslike thermal properties. Fractons have also been reported in single crystals of pure relaxor substances [16,17]. The connection of the local dipole moment caused by the dipole-dipole interaction in relaxors has a fractal structure and it may be the key to explaining the large dielectric response.

The most direct and well-known methods for detecting the BP excitation in actual glassy materials are those used to investigate the v-DOS directly [18–21]: inelastic neutron or x-ray scattering (INS/IXS) and inelastic nuclear scattering. Whereas numerous studies have investigated BPs with low-frequency Raman scattering [3,22–24] and low-temperature specific heat [2,3,25,26], there have been only a few recent THz spectroscopic studies of BP dynamics [27–30]. Theoretical [31–35] and molecular dynamics (MD) simulation [36–39] studies on BPs are also rapidly advancing. On the other hand, relatively few studies have focused on fractons [5,40–42], particularly in the context of nanoscale dynamics, and there are practically no studies of fractons using THz spectroscopy [43]. This is because there is not yet sufficient understanding of the interaction between THz light and the v-DOS in the fracton region, even though there have been numerous THz spectroscopic studies of polymer substances since the late 2000s [44,45].

The THz spectroscopy is more suitable for systematic spectroscopy of a large number of samples than INS/IXS and is superior to Raman scattering for being able to perform spectroscopy on samples that exhibit luminescence with a

*mori@ims.tsukuba.ac.jp

visible light laser. In addition, the absolute values of optical constants such as absorption coefficient can be determined, and this means that if the interaction between THz light and v-DOS is fully understood, then v-DOS information including absolute value can be extracted via THz spectroscopy. For example, the BP frequency as well as the BP intensity can be determined, which would be a strong advantage of THz spectroscopy.

The protein lysozyme is employed in this study as an example of a polymer glasslike substance which might exhibit a BP and fractons in the THz regime. For protein biological function relying on its structural changes, nanoscale long-range vibration is important for revealing the mechanisms of structural dynamics such as oxygen transport [46]. Furthermore, irrespective of the type of protein, proteins universally show a broad v-DOS in the THz region [47], which directly includes the information of elastic heterogeneity in the nanoscale region [31]. Understanding the universal v-DOS is important for elucidating and controlling elastic properties of disordered structural systems. Although a protein molecule is not an actual glassy material, low-frequency Raman scattering has shown [48] that it has glasslike dynamics, even in the case of a single crystal. This suggests that the protein system has an intrinsically disordered and polymeric nature: It can be viewed as a single supramolecule, in which each amino acid and the whole structure of a single protein molecule correspond to a monomer molecule and a polymer chain in a polymer glass, respectively. The availability of structural information about a single crystal of protein from the Protein Data Bank (PDB) makes it possible to discuss the correlation of the fractal structure and its THz dynamics.

In this work, we first formulate the infrared (IR) light-vibration coupling coefficient $C_{IR}(\nu)$ in the fracton region, modifying the $C_{IR}(\nu)$ model proposed by Taraskin *et al.* [49]. We find that the exponent of $C_{IR}(\nu)$ is almost identical to that of the Raman coupling coefficient $C_{Raman}(\nu)$. Second, in the THz spectrum of lysozyme, we observe a BP and fractons and find that the slope of the absorption coefficient in the log-log plot is identical to that of the Raman spectrum. Third, we find that the observed value of the slope in the fracton region is in good agreement with the value predicted by the formalized $C_{IR}(\nu)$ and $C_{Raman}(\nu)$ and is characterized by the fractal and fracton dimensions. Finally, we estimate the structure correlation length associated with the BP and the characteristic wavelengths of the IR and Raman active modes. These results suggest that universal dynamics are present within a single protein molecule.

II. FORMULATION

In this section, we will derive a general formula for $C_{IR}(\nu)$ in the fracton region. First, we briefly introduce the dispersion relation of a fractal system [4,41,50]. In diffusive processes, the mean-squared displacement $\langle R^2 \rangle$ obeys the characteristic law

$$\langle R^2 \rangle \propto t^{2\xi}, \tag{1}$$

where t is time and ξ is a real parameter. In a normal diffusive process, $\xi = 1/2$. For fractal objects, however, the process is more localized, and $\xi < 1/2$. In this case, the autocorrelation

function $P_0(t)$ becomes $P_0(t) \propto t^{-D_f \xi}$, where D_f is the fractal dimension, and we immediately obtain the density of the (fracton) vibrational modes as follows:

$$g(\nu) \propto \nu^{d_f - 1}, \tag{2}$$

where $d_f = 2D^f \xi$ is the fracton dimension. The relation among ξ, D_f, and d_f implies that in the $\xi < 1/2$ case, $d_f < D_f$. Therefore, for a fractal object, the dynamic fracton dimension is generally smaller than the static fractal dimension. In a study by Rammal and Toulouse [50], the dispersion relation of a fractal object with the assumption of length scaling was found to be

$$\nu \propto k^{\frac{D_f}{d_f}}, \tag{3}$$

where k is the wave number. In the present work, we assume that this dispersion relation holds in the fracton region of a protein system. Note that $2\pi k^{-1}$ represents the localized wavelength of the fracton mode rather than the wavelength of a propagating plane wave.

Next, we show how $C_{IR}(\nu)$ behaves in a fractal system by applying the dispersion relation to a universal model proposed by Taraskin *et al.* [49]. $C_{IR}(\nu)$ is generally expressed as [51,52]:

$$C_{IR}(\nu) = \frac{2\pi^2 n}{c\sqrt{\varepsilon_\infty}} \left| \sum_i \frac{q_i}{\sqrt{m_i}} \mathbf{e}_i(\nu) \right|^2, \tag{4}$$

where q_i, m_i, and $\mathbf{e}_i(\nu)$ are the fixed but spatially fluctuating atomic charges, mass, and vibrational eigenvector of frequency ν corresponding to atom i, respectively; ε_∞ represents the high-frequency dielectric constant; and n is the atomic number density. This expression is derived from the linear response theory in the harmonic approximation for atomic vibrations [51]. In the theory of Taraskin *et al.*, q_i is divided into two parts: the uncorrelated, randomly fluctuating charge, q_{1i}, and the correlated charge that satisfies local charge neutrality, q_{2i}. In a crystal system, q_{1i} becomes 0 and $q_{2i} = q_i$. The charge components can then be recast in terms of uncorrelated and correlated charge components (S_1 and S_2, respectively) to simplify Eq. (4):

$$C_{IR}(\nu) = \left\langle \frac{2\pi^2 n}{\overline{m} c \sqrt{\varepsilon_\infty}} \left| \sum_i (q_{1i} + q_{2i}) e^{i\mathbf{k} \cdot \mathbf{r}_i} \right|^2 \right\rangle$$

$$= \frac{2\pi^2 n}{\overline{m} c \sqrt{\varepsilon_\infty}} \langle |S_1 + S_2|^2 \rangle, \tag{5}$$

where $n = \rho / \overline{m}$, ρ is the density, $\overline{m} = N^{-1} \sum_i m_i$ (i runs over atoms) is average mass, and N is the number of atoms in a solid of volume V. If there is no correlation between q_{1i} and q_{2i}, then Eq. (5) reduces to:

$$C_{IR}(\nu) = \frac{2\pi^2 n}{\overline{m} c \sqrt{\varepsilon_\infty}} (\langle |S_1|^2 \rangle + \langle |S_2|^2 \rangle). \tag{6}$$

It is easily found that the first term of Eq. (6) is a constant [49,52]. In the second term, q_{2i} can be considered the result of charge transfers between nearest neighbors, i.e., $q_{2i} = \sum_{j \neq i} \Delta q_{ji}$, where j runs through all the nearest neighbors of atom i and $\Delta q_{ji} = -\Delta q_{ij}$ represents the charge transfer from the originally neutral atom j to the originally neutral atom i.

We assume that we are in the long-wavelength regime [52], and the component S_2 is approximated by the right-hand side of the following equation:

$$S_2 = \left\langle \sum_{(ij)} \Delta q_{ij}(e^{i\mathbf{k}\cdot\mathbf{r}_j} - e^{i\mathbf{k}\cdot\mathbf{r}_i}) \right\rangle$$
$$\simeq k \sum_{(ij)} \Delta q_{ij} e^{i\mathbf{k}\cdot\mathbf{r}_{(ij)}}(i\hat{\mathbf{n}} \cdot \mathbf{r}_{ij}), \tag{7}$$

where $\mathbf{r}_{ij} = \mathbf{r}_j - \mathbf{r}_i$, $\mathbf{r}_{(ij)} = (\mathbf{r}_j + \mathbf{r}_i)/2$ and $\mathbf{k} = k\hat{\mathbf{n}}$. We therefore see that S_2 is proportional to k. When the dispersion relation of the Debye model, i.e., $\nu \propto k$, is substituted into Eq. (7), we obtain a quadratic frequency dependence in the second term of $C_{IR}(\nu)$:

$$\langle |S_2|^2 \rangle \propto k^2 \propto \nu^2. \tag{8}$$

Taraskin's universal functional form of $C_{IR}(\nu)$ in the Debye case then becomes

$$C_{IR}(\nu) = A + B\nu^2. \tag{9}$$

We will now consider the frequency region above the BP frequency [40], where we expect the appearance of *fracton modes*. Rather than the Debye dispersion relation, we insert the Rammal-Toulouse dispersion relation, Eq. (3), into Eq. (7). The second term of $C_{IR}(\nu)$ then becomes

$$\langle |S_2|^2 \rangle \propto k^2 \propto \nu^{2\frac{d_f}{D_f}}, \tag{10}$$

and the frequency exponent changes from 2 to $2d_f/D_f$. We thus obtain the Taraskin form of $C_{IR}(\nu)$ in the fracton region:

$$C_{IR}(\nu) = A + B\nu^{2\frac{d_f}{D_f}}. \tag{11}$$

Considering the behavior of the v-DOS expressed in Eq. (2), we expect the frequency dependence of the absorption coefficient $\alpha(\nu)$ as follows:

$$\alpha(\nu) \propto \nu^{(2d_f/D_f)+d_f-1}. \tag{12}$$

According to Boukenter *et al.* [53], a very similar relation holds in Raman spectroscopy of fractal materials:

$$C_{Raman}(\nu) \propto \nu^{2\frac{d_f d_\phi}{D_f}}. \tag{13}$$

The second term of $C_{IR}(\nu)$ is identical to $C_{Raman}(\nu)$, except for the superlocalized exponent d_ϕ; in many cases, d_ϕ becomes 1. We can therefore expect THz and Raman spectra to show the same gradient in the fracton region.

III. MATERIALS AND METHODS

A. Sample preparation

Lyophilized lysozyme powder from hen egg white at room temperature under atmospheric pressure was used, without further purification. This is a representative global type of single-domain protein with 129 amino acid residues and a molecular weight of 14.3 kDa. The sample used for this study was purchased from Wako Pure Chemical Industries, Ltd. For measurement, a pressure of 1 MPa was applied to the lysozyme powder to prepare a disk-shaped pellet. The THz and Raman spectroscopies for the fracton region were

performed with the same sample subsequent to evacuation in a vacuum chamber for 12 h.

B. Terahertz time-domain spectroscopy

A terahertz time-domain spectroscopy (THz-TDS) system (RT-10000, Tochigi Nikon Co.) and a liquid-helium flow cryostat system (Helitran LT-3B, Advanced Research Systems) [28,30,54,55] were used with the standard transmission configuration for temperature-dependent measurements in the frequency range of 0.25–2.25 THz from 13 to 295 K. Low-temperature grown GaAs photoconductive antennae were used as emitters and detectors of the THz wave. The THz wave propagation path was enclosed in a dry air chamber within which dry air flowed. Another THz-TDS system (TAS7500SU, Advantest Corp.) [28,30,56,57] was used for room-temperature broadband transmission THz spectroscopy. Cherenkov radiation from a lithium niobate single crystal was used as the light source of the THz wave, covering a frequency band of around 0.5–7.0 THz. Asynchronous optical sampling technology was used for detection. To obtain an adequate signal-to-noise ratio in every cycle, 16 384 measurements were performed. The THz wave propagation path was purged with dry air.

C. Low-frequency Raman scattering

Confocal micro-Raman measurements were performed with a depolarized backscattering geometry [58]. A frequency-doubled diode-pumped solid-state Nd:yttrium-aluminium-garnet laser oscillating in a single longitudinal mode at 532 nm (Oxxius LCX-300S) was employed as the excitation source. A homemade microscope with ultra-narrow-band notch filters (OptiGrate) was used to focus the excitation laser and collect the Raman-scattered light. The scattered light was analyzed using a single monochromator (Jovin-Yvon, HR320, 1200 grooves/mm) equipped with a charge-coupled-device camera (Andor, DU420).

D. Maximum entropy method (MEM) analysis of specific heat data

Under the approximation of harmonic vibration, the lattice specific heat $C(T)$ is related to the v-DOS of a solid by the equation:

$$C(T) = 3nk_B \int \frac{x^2 e^x}{(e^x - 1)^2} g(\nu) d\nu, \tag{14}$$

where $x = h\nu/k_B T$. The inverse problem of obtaining $g(\nu)$ from the specific heat data of Ref. [25] was solved using the maximum entropy method (MEM) on specific heat data [59,60] over the temperature range 1.7–23 K. The error in the specific heat data was assumed to be 2%.

IV. RESULTS AND DISCUSSION

A. Boson peak of lysozyme in THz and Raman spectra

In this section, we turn to an actual material, the protein lysozyme, which we studied using THz time-domain spectroscopy and low-frequency Raman spectroscopy, as described under Materials and Methods.
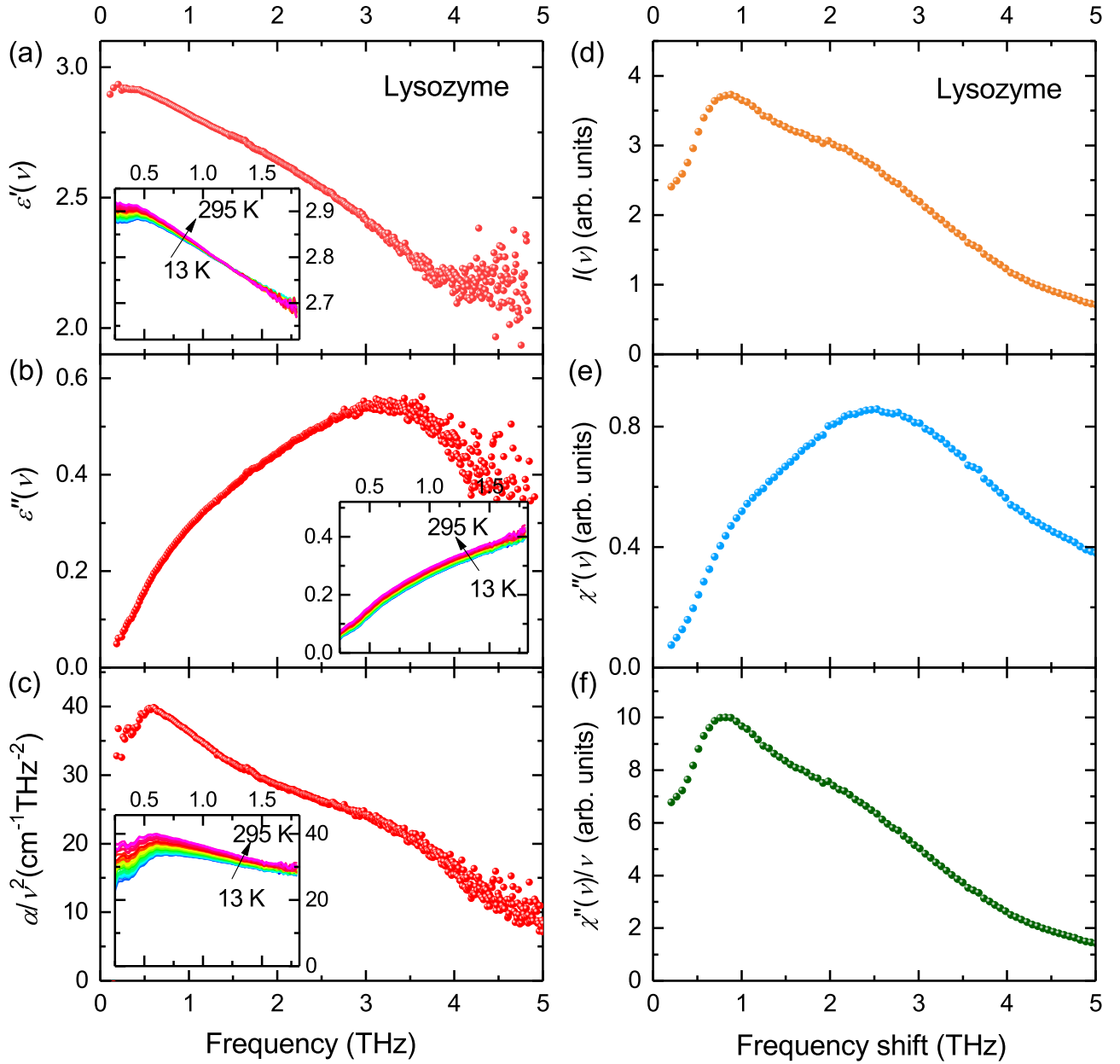
FIG. 1. THz and Raman spectra of lysozyme. (a) Real $\varepsilon'(\nu)$ and (b) imaginary $\varepsilon''(\nu)$ parts of complex dielectric constant, and (c) BP plot $\alpha(\nu)/\nu^2$ of lysozyme determined by THz-TDS measurements at room temperature. Insets of (a), (b), and (c) show temperature dependence of IR spectra, as measured in a heating process with a temperature range of 13 K to 295 K and plotted every 10 K above 20 K. (d) Measured Raman intensity $I(\nu)$ of lysozyme at room temperature. (e) Imaginary part of Raman susceptibility $\chi''(\nu)$. (f) BP plot of Raman spectra $\chi''(\nu)/\nu$. For convenience, 1 THz = 33.3 cm^{-1} = 48 K = 4.14 meV.

Figures 1(a) and 1(b) show, respectively, the real part $\varepsilon'(\nu)$ and the imaginary part $\varepsilon''(\nu)$, of the complex dielectric constant of lysozyme at room temperature. The spectrum of $\varepsilon''(\nu)$ shows a broad absorption band, typical of amorphous materials. A convex upward curve appears > 0.6 THz, rising to a broad peak at 3.26 THz. At first glance, $\varepsilon'(\nu)$ shows Debye relaxation modelike behavior [30], but a close examination of the region around 0.6 THz reveals a small resonance-like peak. These features are more prominent at lower temperatures, as shown in the insets of Figs. 1(a) and 1(b). Similar behavior is generally observed in glassy materials (see Fig. 1 of Ref. [30]). Such a resonance-like deviation

from the conventional Debye relaxation model, suggesting the existence of a BP at around 0.6 THz, is universal in the behavior of the dielectric constant. It results from the characteristic spectral shape of the v-DOS around the BP frequency and from the breakdown of selection rules caused by the disappearance of translational symmetry [30].

To investigate the BP of lysozyme in the IR spectrum, the spectrum of the complex dielectric constant is expressed in terms of $\alpha(\nu)/\nu^2$ (see Appendix). The resulting BP plot of the IR spectrum is shown in Fig. 1(c). The BP of lysozyme is clearly observed at 0.6 THz in the $\alpha(\nu)/\nu^2$ spectrum. We can therefore conclude that detection of the BP using THz

spectroscopy is possible for proteins, as well as for actual glassy materials [30,61].

The BP dynamics of lysozyme have also been investigated using low-frequency Raman scattering. Figure 1(d) shows the measured Raman intensity $I(\nu)$ at room temperature: A clear peak is observed at around 0.8 THz. In general, the Raman susceptibility $\chi''(\nu)$ is extracted from the measured Raman intensity $I(\nu)$ through the following equation [62,63]:

$$I(\nu) = [n_B(\nu, T) + 1]\chi''(\nu), \tag{15}$$

where $n_B(\nu, T) = [\exp(h\nu/k_BT) - 1]^{-1}$ is the Bose-Einstein distribution function. The $\chi''(\nu)$ spectrum obtained is shown in Fig. 1(e) and shows a broad peak at 2.53 THz. We observe that this peak frequency is lower than that of the infrared $\varepsilon''(\nu)$ spectrum (3.26 THz). The ordinate of the BP plot of the Raman spectrum [Fig. 1(f)] is $\chi''(\nu)/\nu$; it is often referred to as reduced intensity. The relation between $\chi''(\nu)$ and $g(\nu)$ is expressed by the following equation [64]:

$$\nu\chi''(\nu) = C_{\text{Raman}}(\nu)g(\nu). \tag{16}$$

For convenience, the BP plot relations are summarized in Appendix.

As shown in Fig. 1(f), in the $\chi''(\nu)/\nu$ spectrum, the BP of the reduced Raman intensity spectrum is observed at around 0.8 THz; this frequency is slightly higher than the BP frequency of the IR spectrum $\nu_{\text{BP-IR}}$, as discussed below. We emphasize that no absorption peak is observed in the $\chi''(\nu)$ spectrum near the BP frequency of the reduced Raman intensity $\nu_{\text{BP-Raman}}$, nor in the $\varepsilon''(\nu)$ IR spectrum [30]. However, as shown in Fig. 1(d), we clearly observe the BP in the measured $I(\nu)$ at room temperature, as we would with a glassy material.

Although room temperature Raman spectroscopy is a well-known method for detecting boson peaks, the peak in the measured $I(\nu)$ at room temperature is not a direct BP derived from a particular mode but a "universal artifact," as discussed in our previous work [30]. At room temperature, k_BT, is approximately six times higher than the typical energy of the BP frequency of 1 THz (cf. 1 THz = 33.3 cm^{-1} = 48 K = 4.14 meV). In the high-temperature approximation, where the thermal factor $n_B(\nu, T) + 1$ of Eq. (15) becomes $1/\nu$, the right-hand side of Eq. (15) transforms into $\chi''(\nu)/\nu$, i.e., the measured $I(\nu)$ at room temperature becomes identical to the BP plot of the Raman spectrum.

B. Comparison among $\varepsilon''(\nu)$, $\chi''(\nu)$, and $g(\nu)$, and determination of coupling coefficients

In this section, we will locate and study the fracton region of lysozyme

We directly compare IR, Raman, and $g(\nu)$ spectra, and determine the light-vibration coupling coefficients, $C_{\text{IR}}(\nu)$ and $C_{\text{Raman}}(\nu)$. Figures 2(a) and 2(b), respectively, show the imaginary parts of $\varepsilon''(\nu)$ and $\chi''(\nu)$ and the BP plots of the IR and Raman spectra on the same axis. From the BP plots shown in Fig. 2(b), we find that $\nu_{\text{BP-Raman}}$ is 1.4 times higher than $\nu_{\text{BP-IR}}$. This difference is phenomenologically attributable to the different frequency dependences of $C_{\text{IR}}(\nu)$ and $C_{\text{Raman}}(\nu)$. It can be seen that there is a perfectly overlapped region of $\varepsilon''(\nu)$ and $\chi''(\nu)$ above the BP frequency, where the convex upward line shapes show the same power-law behavior as
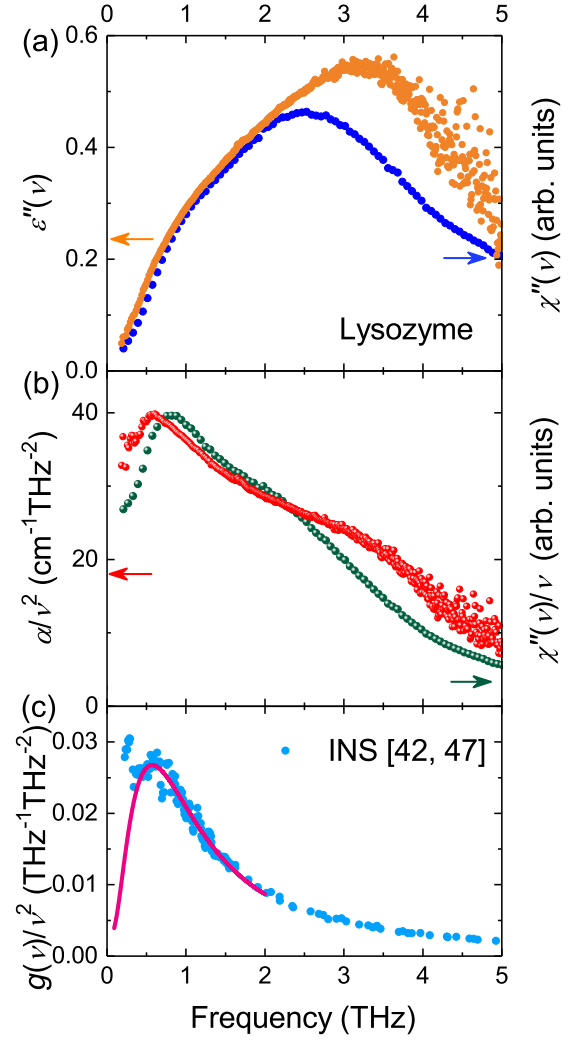

FIG. 2. Comparison of THz, Raman, and v-DOS spectra. (a) Imaginary parts of complex dielectric constant $\varepsilon''(\nu)$ (orange) and Raman susceptibility $\chi''(\nu)$ (blue) of lysozyme. (b) BP plots of IR [$\alpha(\nu)/\nu^2$ (red)] and Raman [$\chi''(\nu)/\nu$ (green)] spectra. (c) BP plot of v-DOS $g(\nu)/\nu^2$. The data of $g(\nu)$ are quoted from previous studies based on INS [42,47]. The log-normal fit used to obtain the BP frequency is shown by the pink curve.

expected in the fracton region. To ascertain that this behavior is indeed exponential and the same for both, we create a log-log plot of $\varepsilon''(\nu)$ and $\chi''(\nu)$, as shown in Fig. 4(a). In the region from around 0.8 THz up to 2.2 THz, the two curves are linear and nearly identical; this frequency range constitutes the fracton region.

To evaluate the interaction between light and v-DOS $g(\nu)$ in the BP and fracton regions, we determine $C_{\text{IR}}(\nu)$ and $C_{\text{Raman}}(\nu)$ by combining $g(\nu)$ data obtained from the results of INS measurements [42,47] with our data for $\varepsilon''(\nu)$ and $\chi''(\nu)$. The $g(\nu)$ and BP plots $g(\nu)/\nu^2$ are shown in Figs. 4(a) and 2(c), respectively. Furthermore, to obtain the absolute value of $C_{\text{IR}}(\nu)$, we determine the absolute value of $g(\nu)$ by fitting low-temperature specific heat data [25] by the MEM. (For further details, see Fig. 3.) In the $g(\nu)/\nu^2$ spectrum shown in Fig. 2(c), we find that the BP frequency $\nu_{\text{BP-INS}}$ is 0.58 THz, obtained via log-normal function fitting [65]. In the
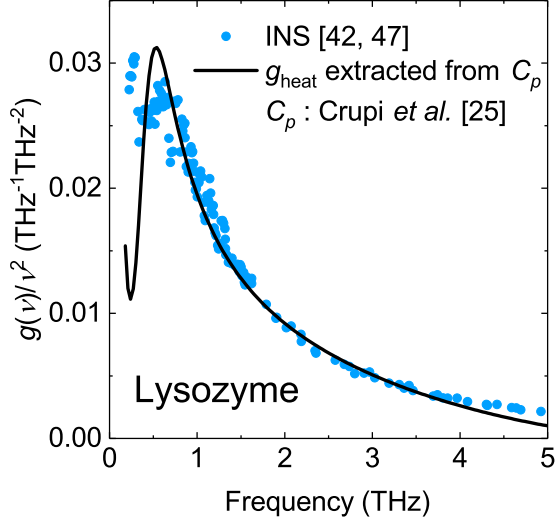
FIG. 3. Adjustment of $g(\nu)$ by inelastic neutron scattering with the absolute value determined by performing MEM analysis on the low-temperature specific heat (C_p) data of the lysozyme. We depicted and connected $g(\nu)$ from inelastic neutron scattering measurements by Perticaroli *et al.* [47] and Lushnikov *et al.* [42] for achieving higher accuracy of $g(\nu)$ [47] in the BP region and $g(\nu)$ [42] in the fracton region. Based on data depicted from the results of low-temperature specific heat measurements reported in the work by Crupi *et al.* [25], the specific heat v-DOS as $g_{\text{heat}}(\nu)$ was extracted by MEM analysis. We determined the absolute value of the $g_{\text{INS}}(\nu)$ used in this work through conformation with the absolute value of $g_{\text{heat}}(\nu)$ at the BP frequency.

log-log plot of $g(\nu)$ shown in Fig. 4(a), $\nu_{\text{BP−INS}}$ becomes a boundary where the upper and lower regions show different gradients of power-law dependence. Generally, below the BP frequency, v-DOS becomes proportional to ν^{D-1}, where $D = 3$, indicating that the v-DOS follows the Debye model of the three-dimensional (3D) system, and the $g(\nu)$ of lysozyme also shows similar behavior below $\nu_{\text{BP−INS}}$. In contrast, above $\nu_{\text{BP−INS}}$, the value of the exponent decreases to 0.4, which is expected in the fracton region where the exponent is expressed [4] as $d_f - 1$. Then $C_{\text{IR}}(\nu)$ with the absolute value is experimentally determined through the following relation [66]:

$$\alpha(\nu) = C_{\text{IR}}(\nu)g(\nu). \tag{17}$$

In the same way, $C_{\text{Raman}}(\nu)$ of lysozyme is determined by Eq. (16). The results are shown in Fig. 4(b) and its inset. The related equations are summarized in Appendix.

C. Analysis of coupling coefficients: Boson peak

The $C_{\text{IR}}(\nu)$ in the vicinity of the BP frequency has been evaluated quantitatively using Taraskin's model [49]. On the other hand, $C_{\text{Raman}}(\nu)$ has been explained by the coupling of light with elastic strains via spatially fluctuating elasto-optic constants [67]. In the following, we focus mainly on $C_{\text{IR}}(\nu)$.

First, we focus on the behavior of $C_{\text{IR}}(\nu)$ and $C_{\text{Raman}}(\nu)$ around the BP frequency, as shown in the inset of Fig. 4(b). Although the peak structure of BP in $g(\nu)$ is unclear, a difference in the frequency dependence of the $C_{\text{IR}}(\nu)$ and $C_{\text{Raman}}(\nu)$ around the BP frequency have been observed. In the
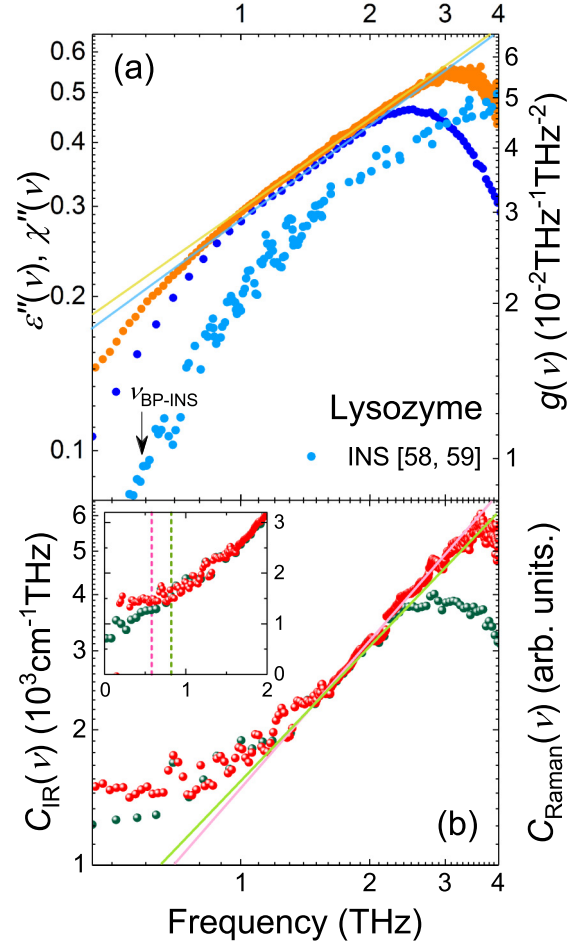

FIG. 4. Log-log plot of THz, Raman, and v-DOS spectra and coupling coefficients. (a) Log-log plot of imaginary parts of complex dielectric constant $\varepsilon''(\nu)$ (orange), Raman susceptibility $\chi''(\nu)$ (arb. units) (blue), and v-DOS $g(\nu)$ (cyan) of lysozyme. $g(\nu)$ data are quoted from previous studies based on INS [42,47]. (b) IR light-vibration (red) and Raman (green) coupling coefficients [$C_{\text{IR}}(\nu)$ and $C_{\text{Raman}}(\nu)$] of lysozyme in the log-log representation. The inset shows the linear representation of $C_{\text{IR}}(\nu)$ and $C_{\text{Raman}}(\nu)$ in the vicinity of the BP frequency.

vicinity of the BP frequency, the $C_{\text{IR}}(\nu)$ of lysozyme consists of a constant term and a quadratic or higher-order term. Like silica glass [49,61], lysozyme has a $C_{\text{IR}}(\nu)$ dominated by a constant term below the BP frequency. In contrast, the $C_{\text{Raman}}(\nu)$ of lysozyme shows an almost linear frequency dependence, which is characteristic of glassy substances [24]. As a result, $\nu_{\text{BP−IR}}$ is almost the same as $\nu_{\text{BP−INS}}$, while $\nu_{\text{BP−Raman}}$ becomes slightly higher than $\nu_{\text{BP−INS}}$.

In the following, we analyze the frequency dependence and absolute value of $C_{\text{IR}}(\nu)$. As we have seen, for glassy materials, Taraskin *et al.* derived a universal functional form for the $C_{\text{IR}}(\nu)$ [49,52] by applying linear response theory. The result is given by Eq. (9), where the constant term A originates from the response of the uncorrelated charge q_1, i.e., of the randomly fluctuating charges that deviate from the average charge of each atom. The higher-order term B, which plays a dominant role above the BP frequency, is related to q_2, the average charge value. Applying Taraskin's model

TABLE I. Top: Parameters used for the calculation of uncorrelated charge q_1 in $C_{IR}(\nu)$ for the lysozyme. Experimentally determined constant term A, average mass $\overline{m}$, density ρ, and dielectric constant at 0.8 THz instead of the high-frequency dielectric constant ε_∞ and obtained uncorrelated charge q_1 for the lysozyme. Bottom: Comparison between lysozyme and silica glass. The data of the silica glass were measured separately and the values are consistent with a previous report [49,61].

	A (cm^{-1}THz)	$\overline{m}$ (g)	ρ (gcm^{-3})	ε_∞	$q_1(e)$
Lysozyme	1.4×10^3	1.28×10^{-23}	0.87	2.19	0.13

	Lysozyme	Silica glass	Comparison with silica (Lys/Silica)
α(cm^{-1})	25 (at 0.8 THz)	1.8 (at 1 THz)	14
A (cm^{-1}THz)	1.4×10^3	9.0×10^2	16
$q_1(e)$	0.13	0.06	2.1
$\overline{m}$ (10^{-23}g)	1.28	3.37	0.38
ρ (gcm^{-3})	0.87	2.21	0.39
ε_∞	2.19	3.81	0.57
$\frac{2\pi^2\rho}{\overline{m}^2 c\sqrt{\varepsilon_\infty}}$			3.6

to lysozyme, we find the value of A, which is dominant in the vicinity of the BP frequency, to be 1.4×10^3 cm^{-1} THz. We then use the following relation from Taraskin's model to evaluate the uncorrelated charge q_1:

$$A = \frac{\langle q_{1i}^2 \rangle 2\pi^2 n}{\overline{m} c \sqrt{\varepsilon_\infty}}. \qquad (18)$$

From this, we determine the q_1 of lysozyme to be 0.13 e, and other parameters are listed in Table I. At 1 THz, the absorption coefficient of lysozyme is 21 times greater than that of silica glass [49,61], which is a typical network glass-former (see Table I), while the A of lysozyme is 16 times greater than that of silica glass [49,61]. This result suggests that the large $C_{IR}(\nu)$ is responsible for lysozyme's large absorption in the THz region. Let us further consider the origin of this large $C_{IR}(\nu)$. The uncorrelated charge q_1 of lysozyme is 2.1 times larger than that of silica glass; the contribution of the uncorrelated charge term $\langle q_{1i}^2 \rangle$ is thus 4.5 times larger. In addition, the average mass, $\overline{m}$, of lysozyme is 0.38 times smaller than that of silica glass. As a result, the affective term, $\overline{m}^{-2}$, becomes 6.9 times larger and makes a larger contribution compared to the uncorrelated charge. Therefore, an organic glass-former with a relatively low mass generally shows a larger constant term A in the vicinity of the BP frequency than an inorganic material; this is a result of the organic glass's lower mass, independent of the effect of uncorrelated charge.

D. Analysis of coupling coefficients: Fracton

Next, we shed light on the fracton behavior that appears above the BP frequency, where both $\varepsilon''(\nu)$ and $\chi''(\nu)$ exhibit a power-law behavior, as shown in Fig. 4(a). This is because both the v-DOS and coupling coefficients also show a power-law behavior.

As shown in Fig. 4(a), $\varepsilon''(\nu)$ and $\chi''(\nu)$ exhibit linear frequency dependence above the BP frequency in the log-log representation. Interestingly, and as expected, the IR and Raman spectra share a frequency region with almost identical

slopes, which extends up to 2.53 THz. Above that frequency, the Raman spectrum departs from linearity and eventually begins to fall. The IR spectrum, however, remains linear to 3.26 THz. The v-DOS ($g(\nu)$) [42,47] is plotted in the same figure to show the fracton region directly. The $g(\nu)$ also shows linearity above 1.7 THz, although the starting frequency is slightly higher than for IR and Raman spectra. Such power-law behaviors of both the IR and Raman spectra and the v-DOS spectrum generate linear regions in both $C_{IR}(\nu)$ and $C_{Raman}(\nu)$. These linear regions are the fracton regions. The exponent values for $C_{IR}(\nu)$ and $C_{Raman}(\nu)$ are 1.10 and 1.00, respectively (see the left column of Table II), obtained from the fit in Fig. 4(b). These exponent values are what we expect to be represented by $2d_f/D_f$ in this study.

Here we examine whether the measured slope of $C_{IR}(\nu)$ obtained by our method agrees with the value of $2d_f/D_f$ when D_f and d_f are found by other theoretical and experimental methods.

First, we calculate the mass fractal dimension of lysozyme as $D_{f-calc} = 2.75$, using structural information about lysozyme (1LYZ) obtained from the PDB. The method is illustrated in Figs. 5(a) and 5(b). D_{f-calc} is defined as the slope obtained when plotting the mass of all atoms contained in concentric spheres of radius R around the center of gravity of the lysozyme molecule on a log-log scale [68]. Our value of D_{f-calc} so obtained is consistent with that reported previously [68]. The value of the fracton dimension $d_{f-calc} = 1.43$ is taken from the literature, where the harmonic spectrum of the vibrational modes (calculated by a Gaussian network model) was used to determine the fracton dimension for a protein containing approximately 100 amino acids [69]. By

TABLE II. Exponent values of $C_{IR}(\nu)$ and $C_{Raman}(\nu)$ in the fracton region. Fitting lines are shown in Fig. 4(b).

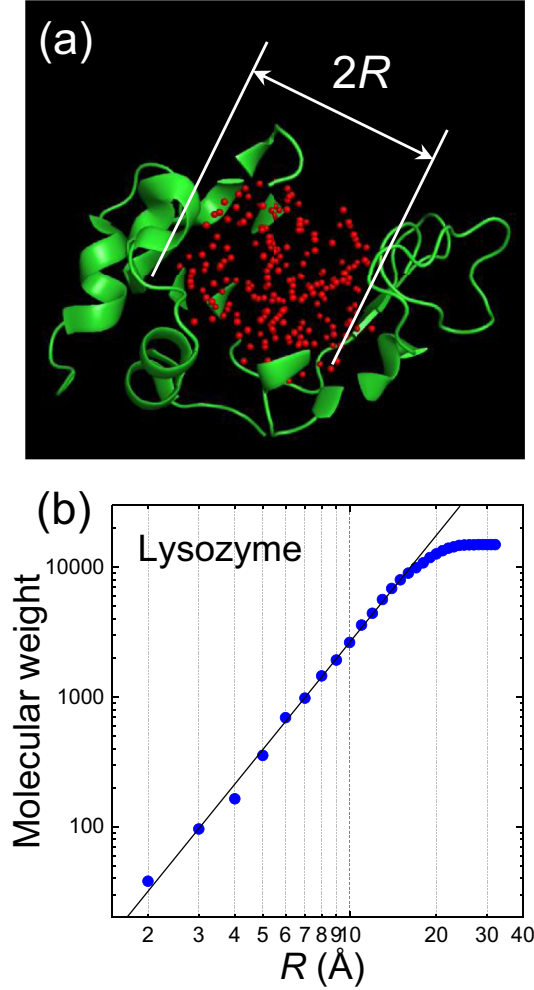|	Exponent value of $C_{IR}(\nu)$ and $C_{Raman}(\nu)$
IR	1.10
Raman	1.00

FIG. 5. Calculation of mass fractal dimension of lysozyme molecule. (a) Atoms (red balls) contained in a sphere of radius R around the center of gravity of the lysozyme molecule. For the lysozyme atomic coordinate arrangement, information on 1LYZ was taken from the PDB. (b) Log-log plot of the R dependence of molecular weight contained in a sphere of radius R around the center of gravity of lysozyme. When the diameter of the sphere exceeds the diameter of the lysozyme molecules, the molecular weight levels off. From fitting to the linear region, the mass fractal dimension of the lysozyme molecule was found to be $D_{f-\text{calc}} = 2.75$.

substituting $D_{f-\text{calc}}$ and $d_{f-\text{calc}}$ into the $C_{\text{IR}}(\nu)$ formula, the calculated slope of $C_{\text{IR}}(\nu)$ is $2d_{f-\text{calc}}/D_{f-\text{calc}} = 1.04$, in good agreement with our experimental value of 1.10 (see Table III).

Second, we consider the values of $D_{f-\text{exp}}$ and $d_{f-\text{exp}}$ which have been experimentally determined via small angle neutron scattering (SANS) and INS [42], respectively. The fractal dimension, $D_{f-\text{exp}} = 2.78$, of lysozyme is obtained from the power-law dependence of the SANS intensity on the wave number in the double logarithmic scale within a spatial region of 2.6–4.4 nm. The existence of such a power law suggests that the mass fractal of lysozyme appears within a single lysozyme molecule with a diameter of approximately 3.7 nm [70]. The fracton dimension, $d_{f-\text{exp}} = 1.43$, of lysozyme is obtained from the v-DOS determined by the INS experiment [42]. This v-DOS consists of two linear segments with slopes

TABLE III. Numerically ($D_{f-\text{calc}}$ and $d_{f-\text{calc}}$) and experimentally ($D_{f-\text{exp}}$ and $d_{f-\text{exp}}$) obtained fractal and fracton dimensions and calculated $2d_f/D_f$. A fitting line to extract $D_{f-\text{calc}}$ is shown in Fig. 5(b).

	D_f	d_f	$2d_f/D_f$
Calculation	2.75	1.43[a]	1.04
Experiment	2.78[b]	1.43[c]	1.02

[a]Reference [69].
[b]Reference [42].
[c]Reference [42].

of 1.99 and 0.43, below and above the BP frequency, respectively, with the BP as the boundary. The former is in good agreement with the behavior of the 3D Debye model. The latter corresponds to the value of $d_f - 1$, i.e., to fracton behavior of the v-DOS. Using these values, the slope of $C_{\text{IR}}(\nu)$ is calculated as $2d_{f-\text{exp}}/D_{f-\text{exp}} = 1.02$. This result is also in good agreement with our experimentally determined slope of 1.10. Thus, we have confirmed the validity of the proposed $C_{\text{IR}}(\nu)$ in the fracton region by two independent methods.

We can quantitatively describe the slope of the absorption coefficient $\alpha(\nu)$ observed in experimental data using the $C_{\text{IR}}(\nu)$ formula of the fracton region. The results show that the concept of the fracton is adequate for expressing the observed power-law behavior of the region above the BP frequency of the protein lysozyme in the IR and Raman spectra. Even though we conducted these tests only on the protein lysozyme, our results are applicable not only to other proteins but also universally to other polymeric glasses with a fractal structure.

E. Hypothetical dispersion relation and characteristic lengths

Finally, by considering the dispersion relation used for the coupling coefficient, we discuss the end mode of the fracton region. Equation (17) is approximated in terms of acoustic modes as $\alpha(\nu) = \sum C_i(\nu)g_i(\nu) = C_{\text{LA}}(\nu)g_{\text{LA}}(\nu) + C_{\text{TA}}(\nu)g_{\text{TA}}(\nu) + \text{other terms}$ [66]. Generally, the transverse acoustic (TA) mode plays a dominant role in the vicinity of the BP frequency. This is because the slope of the dispersion relation is smaller in the TA mode than in the longitudinal acoustic (LA) mode, resulting in a larger v-DOS. We also note that neither $\alpha(\nu)$ nor $g(\nu)$ show any jumps in the vicinity of the BP in our system. Therefore, we propose the following hypothesis: $2\pi\nu = V_{\text{TA}}k$ and $\nu \propto k^{\frac{D_f}{d_f}}$ are continuous at the BP. (Here V_{TA} is the sound velocity of the TA mode. We also specify that the contribution of the LA mode is neglected.) Defining $\hat{\nu} = \nu/\nu_{\text{BP}}$, $\hat{k} = k/k_{\text{BP}}$, $2\pi\nu_{\text{BP}} = V_{\text{TA}}k_{\text{BP}}$, the dispersion relation becomes

$$\begin{cases} \hat{\nu} = \hat{k} & k < k_{\text{BP}} \\ \hat{\nu} = \hat{k}^{\frac{D_f}{d_f}} & k > k_{\text{BP}} \end{cases}, \quad (19)$$

and the coupling coefficient becomes

$$C_{\text{IR}}(\nu) = \begin{cases} A + B\nu_{\text{BP}}^2\hat{\nu}^2 & \nu < \nu_{\text{BP}} \\ A + B\nu_{\text{BP}}^2\hat{\nu}^{2\frac{d_f}{D_f}} & \nu > \nu_{\text{BP}} \end{cases}. \quad (20)$$

It is obvious that $C_{\text{IR}}(\nu)$ is continuous at the BP. At $k = k_{\text{BP}}$, it is necessary that k is not differentiable but continuous.
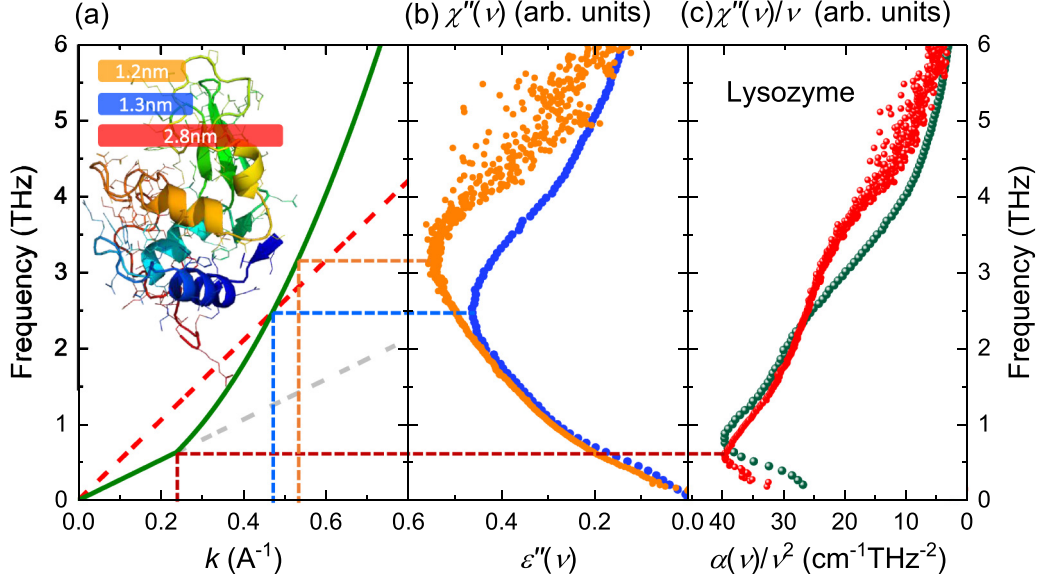
FIG. 6. Dispersion relation in fracton region and THz and Raman spectra. (a) Dispersion relation of TA and fracton modes of lysozyme with the hypothesis of continuous connection at the BP frequency (green solid line). The LA (red dashed line) and TA (gray dashed line) modes are also shown, with sound velocity as measured by Perticaroli *et al.* [47] The dotted lines represent the structure correlation length (wine red dashed line) and the characteristic wavelengths (blue (Raman) and orange (IR) dashed lines). The values of these lengths are indicated by bars on the figure of the lysozyme molecule. (b) Imaginary parts of complex dielectric constant $\varepsilon''(\nu)$ (orange) and Raman susceptibility $\chi''(\nu)$ (blue) of lysozyme. (c) BP plots of IR [$\alpha(\nu)/\nu^2$ (red)] and Raman [$\chi''(\nu)/\nu$ (green)] spectra.

Based on this hypothetical dispersion relation, we now discuss estimation of the correlation length for the BP mode, and characteristic lengths for the end of the fracton.

Figure 6(a) shows the dispersion relations described by the equations:

$$2\pi \nu = V_{\text{TA}} k, \tag{21}$$

and

$$2\pi \nu = V_{\text{TA}} k_{\text{BP}}^{1-\frac{D_f}{d_f}} k^{\frac{D_f}{d_f}}. \tag{22}$$

The sound velocities of lysozyme in the TA mode and the LA mode at 300 K are $V_{\text{TA}} = 1.70 \times 10^3 \, \text{m/s}$ and $V_{\text{LA}} = 3.31 \times 10^3 \, \text{m/s}$, determined through Brillouin measurements in a study by Perticaroli *et al.* [47]. As the fracton dispersion relation indicated by Eq. (22) has an exponent of $D_f/d_f > 1$, it shows an exponential function with an upward curve (with a larger monotone increasing rate) compared with the dispersion relation of the TA mode. At the BP frequency, due to the end frequency of the dispersion relation of the TA mode, the correlation length for the BP of lysozyme, ξ_{BP} [see Figs. 6(a) and 6(c)], is estimated to be 2.8 nm according to the relation $\xi_{\text{BP}} \approx V_{\text{TA}}/\nu_{\text{BP}}$; this represents the size distribution of the lowest-energy vibrational mode localized in a blob [71]. This is smaller than the hydrodynamic diameter of a single lysozyme molecule, $d_{\text{LYS}} = 3.7 \, \text{nm}$ [70], and larger than the average size of an amino acid residue (approximately 0.4 nm) [72]. This correlation length indicates a distance that contains approximately 7 amino acids, and corresponds to the volume of a sphere containing 180 amino acids within radius $R = \xi_{\text{BP}}$ from the center of gravity.

The fact that $\xi_{\text{BP}} < d_{\text{LYS}}$ suggests that the origin of the BP in the protein is the intrinsic disorder inside a single protein molecule rather than the disordered arrangement of the protein molecules with respect to each other. In addition, we point out that the structure of proteins is similar to that of polymer glasses, and that both exhibit boson peaks. In general, a polymer glass is a substance with a chain structure produced through the covalent bonding of monomer molecules. Recent molecular dynamics (MD) simulations have shown that the BP frequencies of monomer and polymer glasses do not differ fundamentally; they are determined by the noncovalent bonds that exist between all monomers, and not by the covalent bonds that connect the monomers [73–75]. In proteins, there are several kinds of noncovalent bonds with different magnitudes of force, such as weak van der Waals bonds and hydrogen bonds, and their complexity makes it difficult to extract the intrinsic determinant factor of BPs. The study by Perticaroli *et al.* [47] pointed out the relation between the BP frequency and the size of the secondary structure; however, quantitative understanding of the determinants of BP frequency in protein systems remains an unsolved problem.

Finally, we discuss the end mode of the fracton using the dispersion relation above the BP frequency. Recent MD simulation studies have shown v-DOS behavior in the low-frequency range of polymer glasses [73–75]. In the study by Milkus *et al.*, the broad peak of the v-DOS from low-frequency noncovalent vibration modes is referred to as the Lennard-Jones (LJ) sea [73]. These vibrations are classified according to their direction with respect to the polymer chain: there are an along-chain, a perpendicular component, and an out-of-plane rocking motion. Then, in the LJ sea, the v-DOS peak of the along-chain motion is shown to appear

at a lower frequency than that of the perpendicular motion. Here we speculate that the peaks of the along-chain motion and perpendicular motion bands shown in the MD calculation correspond to the peak of 2.53 THz in the Raman active $\chi''(\nu)$ and the peak of 3.26 THz in the IR active $\varepsilon''(\nu)$, respectively. Furthermore, the wavelength of the mode at each peak frequency of $\varepsilon''(\nu)$ and $\chi''(\nu)$ can be estimated by considering the dispersion relation of the fracton [see Figs. 6(a) and 6(b)]. The size of the end mode of the fracton in the Raman spectrum is 1.32 nm, which corresponds to a distance containing approximately 3.3 amino acids. In contrast, the IR active mode has a size of 1.16 nm, which corresponds to a distance containing 2.9 amino acids. Finally, we discuss the end mode of the fracton in the v-DOS spectrum. In the v-DOS spectrum observed by Lushnikov *et al.*, the end of the fracton region is around 7.1 THz [76]. We find the size of the end mode to be 0.79 nm, corresponding to the size of approximately 2 amino acids. From our discussion of the size of the fracton mode, we conclude that the vibration of the fracton region results from the self-similar structure of the amino acid molecule and the noncovalent vibrational modes. Further, in the recent MD simulation of polymer glass [75], the result did not show the fractal structure in the scale of correlation length, and fracton did not appear in the v-DOS, which was calculated from the simple Kremer-Grest bead-spring model. The verification of our hypothesis about the continuity of the dispersion relation is a future work by combining experiments and MD simulation. Especially in MD simulation, it will be required that the entire structure shows both fractal and the fracton appear in the v-DOS.

V. CONCLUSIONS

This study has shown that universal excitations in disordered systems, such as boson peaks and fractons, are detectable by THz spectroscopy. For detection of fractons, we found the IR light-vibration coupling coefficient, $C_{\mathrm{IR}}(\nu)$, in the fracton region by combining the $C_{\mathrm{IR}}(\nu)$ model for disordered systems proposed by Taraskin *et al.* [49] with the fracton theory proposed by Alexander and Orbach [4]. We found that the $C_{\mathrm{IR}}(\nu)$ and $C_{\mathrm{Raman}}(\nu)$ in the fracton region are almost identical, and exhibit the exponent $2d_f/D_f$. To verify $C_{\mathrm{IR}}(\nu)$, we performed THz time-domain and low-frequency Raman spectroscopies on the protein lysozyme, which is essentially

a single disordered and self-similar supramolecule. The exponents of coupling coefficients were successfully explained using the values of fractal and fracton dimensions. By assuming the continuity of the dispersion relation between the TA mode and the fracton, we concluded that the fracton originates from the self-similarity of the structure of the amino acids of a single protein molecule. The fact that THz light can capture the BP and fracton will be important for understanding these universal dynamics in the nanoscale regions of disordered systems.

APPENDIX

The summary of BP plot relations for IR spectra is as follows:

$$\alpha(\nu) = C_{\mathrm{IR}} g(\nu), \tag{A1a}$$

$$\frac{\alpha(\nu)}{\nu} = C_{\mathrm{IR}} \frac{g(\nu)}{\nu} = \frac{2\pi\mu'}{cn(\nu)}\varepsilon''(\nu) = \frac{4\pi}{c}\kappa(\nu), \tag{A1b}$$

$$\frac{\alpha(\nu)}{\nu^2} = C_{\mathrm{IR}} \frac{g(\nu)}{\nu^2}, \tag{A1c}$$

where μ' is the real part of permeability, $n(\nu)$ is the refractive index, and $\kappa(\nu)$ is the extinction coefficient.

Summary of BP plot relations for Raman spectra are following. The rightmost parts of Eqs. (A2a), (A2b), and (A2c) represent the high-temperature approximation of Raman spectra.

$$\nu\chi''(\nu) = C_{\mathrm{Raman}}(\nu)g(\nu) = \frac{\nu I(\nu)}{n_B(\nu,T)+1} \approx \nu^2 I(\nu), \tag{A2a}$$

$$\chi''(\nu) = C_{\mathrm{Raman}}(\nu)\frac{g(\nu)}{\nu} = \frac{I(\nu)}{n_B(\nu,T)+1} \approx \nu I(\nu), \tag{A2b}$$

$$\frac{\chi''(\nu)}{\nu} = C_{\mathrm{Raman}}(\nu)\frac{g(\nu)}{\nu^2} = \frac{I(\nu)}{\nu[n_B(\nu,T)+1]} \approx I(\nu). \tag{A2c}$$

[1] T. Nakayama, Rep. Prog. Phys. **65**, 1195 (2002).

[2] R. C. Zeller and R. O. Pohl, Phys. Rev. B **4**, 2029 (1971).

[3] W. A. Phillips, *Amorphous Solids: Low-Temperature Properties* (Springer, Berlin, 1981).

[4] S. Alexander and R. Orbach, J. Phys. (Paris) **43**, 625 (1982).

[5] T. Nakayama, K. Yakubo, and R. L. Orbach, Rev. Mod. Phys. **66**, 381 (1994).

[6] B. C. Sales, B. C. Chakoumakos, R. Jin, J. R. Thompson, and D. Mandrus, Phys. Rev. B **63**, 245113 (2001).

[7] T. Mori, K. Iwamoto, S. Kushibiki, H. Honda, H. Matsumoto, N. Toyota, M. A. Avila, K. Suekuni, and T. Takabatake, Phys. Rev. Lett. **106**, 015501 (2011).

[8] T. Takabatake, K. Suekuni, T. Nakayama, and E. Kaneshita, Rev. Mod. Phys. **86**, 669 (2014).

[9] K. Suekuni, C. H. Lee, H. I. Tanaka, E. Nishibori, A. Nakamura, H. Kasai, H. Mori, H. Usui, M. Ochi, T. Hasegawa, M. Nakamura, S. Ohira-Kawamura, T. Kikuchi, K. Kaneko, H. Nishiate, K. Hashikuni, Y. Kosaka, K. Kuroki, and T. Takabatake, Adv. Mater. **30**, 1706230 (2018).

[10] M. Tachibana and E. Takayama-Muromachi, Phys. Rev. B **79**, 100104(R) (2009).

[11] J. F. Gebbia, M. A. Ramos, D. Szewczyk, A. Jezowski, A. I. Krivchikov, Y. V. Horbatenko, T. Guidi, F. J. Bermejo, and J. L. Tamarit, Phys. Rev. Lett. **119**, 215506 (2017).

[12] M. Moratalla, J. F. Gebbia, M. A. Ramos, L. C. Pardo, S. Mukhopadhyay, S. Rudić, F. Fernandez-Alonso, F. J. Bermejo, and J. L. Tamarit, Phys. Rev. B **99**, 024301 (2019).

[13] Y. Liu, Q. Xi, J. Zhou, T. Nakayama, and B. Li, Phys. Rev. B **93**, 214305 (2016).

[14] T. Tadano and S. Tsuneyuki, Phys. Rev. Lett. **120**, 105901 (2018).

[15] M. Baggioli and A. Zaccone, Phys. Rev. Lett. **122**, 145501 (2019).

[16] A. Koreeda, H. Taniguchi, S. Saikan, and M. Itoh, Phys. Rev. Lett. **109**, 197601 (2012).

[17] S. Tsukada, K. Ohwada, H. Ohwa, S. Mori, S. Kojima, N. Yasuda, H. Terauchi, and Y. Akishige, Sci. Rep. **7**, 17508 (2017).

[18] U. Buchenau, M. Prager, N. Nücker, A. J. Dianoux, N. Ahmad, and W. A. Phillips, Phys. Rev. B. **34**, 5665 (1986).

[19] B. Rufflé, D. A. Parshin, E. Courtens, and R. Vacher, Phys. Rev. Lett. **100**, 015501 (2008).

[20] G. Baldi, V. M. Giordano, G. Monaco, and B. Ruta, Phys. Rev. Lett. **104**, 195501 (2010).

[21] A. I. Chumakov, G. Monaco, A. Monaco, W. A. Crichton, A. Bosak, R. Ruffer, A. Meyer, F. Kargl, L. Comez, D. Fioretto, H. Giefers, S. Roitsch, G. Wortmann, M. H. Manghnani, A. Hushur, Q. Williams, J. Balogh, K. Parliński, P. Jochym, and P. Piekarz, Phys. Rev. Lett. **106**, 225501 (2011).

[22] V. K. Malinovsky and A. P. Sokolov, Solid State Commun. **57**, 757 (1986).

[23] S. Kojima, Phys. Rev. B **47**, 2924 (1993).

[24] N. V. Surovtsev and A. P. Sokolov, Phys. Rev. B **66**, 054205 (2002).

[25] C. Crupi, G. D'Angeloa, U. Wanderlingh, V. C. Nibali, and C. Vasi, Spectroscopy **24**, 201 (2010).

[26] G. C. Jr., G. Carini, D. Cosio, G. D'Angelo, and F. Rossi, Philos. Mag. **96**, 761 (2016).

[27] M. Naftaly and R. E. Miles, J. Non. Cryst. Solids **351**, 3341 (2005).

[28] T. Shibata, T. Mori, and S. Kojima, Spectrochim. Acta A **150**, 207 (2015).

[29] J. Sibik and J. A. Zeitler, Philos. Mag. **96**, 842 (2016).

[30] M. Kabeya, T. Mori, Y. Fujii, A. Koreeda, B. W. Lee, J. H. Ko, and S. Kojima, Phys. Rev. B **94**, 224204 (2016).

[31] W. Schirmacher, Europhys. Lett. **73**, 892 (2006).

[32] W. Schirmacher, G. Ruocco, and T. Scopigno, Phys. Rev. Lett. **98**, 025501 (2007).

[33] M. Wyart, Europhys. Lett. **89**, 64001 (2010).

[34] E. Degiuli, A. Laversanne-Finot, G. Düring, E. Lerner, and M. Wyart, Soft Matter **10**, 5628 (2014).

[35] S. Franz, G. Parisi, P. Urbani, and F. Zamponi, Proc. Natl. Acad. Sci. U.S.A. **112**, 14539 (2015).

[36] H. Shintani and H. Tanaka, Nat. Mater. **7**, 870 (2008).

[37] A. Tanguy, B. Mantisi, and M. Tsamados, Europhys. Lett. **90**, 16004 (2010).

[38] E. Lerner, G. Düring, and E. Bouchbinder, Phys. Rev. Lett. **117**, 035501 (2016).

[39] H. Mizuno, H. Shiba, and A. Ikeda, Proc. Natl. Acad. Sci. U.S.A. **114**, E9767 (2017).

[40] S. Saikan, T. Kishida, Y. Kanematsu, H. Aota, A. Harada, and M. Kamachi, Chem. Phys. Lett. **166**, 358 (1990).

[41] X. Yu and D. M. Leitner, J. Chem. Phys. **119**, 12673 (2003).

[42] S. G. Lushnikov, A. V. Svanidze, S. N. Gvasaliya, G. Torok, L. Rosta, and I. L. Sashin, Phys. Rev. E **79**, 031913 (2009).

[43] T. Ohsaka and T. Ihara, Phys. Rev. B **50**, 9569 (1994).

[44] S. Wietzke, C. Jansen, M. Reuter, T. Jung, D. Kraft, S. Chatterjee, B. M. Fischer, and M. Koch, J. Mol. Struct. **1006**, 41 (2011).

[45] H. Hoshina, S. Ishii, S. Yamamoto, Y. Morisawa, H. Sato, T. Uchiyama, Y. Ozaki, and C. Otani, IEEE Trans. Terahertz Sci. Technol. **3**, 248 (2013).

[46] G. Acbas, K. A. Niessen, E. H. Snell, and A. G. Markelz, Nat. Commun. **5**, 3076 (2014).

[47] S. Perticaroli, J. D. Nickels, G. Ehlers, and A. P. Sokolov, Biophys J. **106**, 2667 (2014).

[48] H. Urabe, Y. Sugawara, M. Ataka, and A. Rupprecht, Biophys. J. **74**, 1533 (1998).

[49] S. N. Taraskin, S. I. Simdyankin, S. R. Elliott, J. R. Neilson, and T. Lo, Phys. Rev. Lett. **97**, 055504 (2006).

[50] R. Rammal and G. Toulouse, J. Phys. (Paris) **44**, 13 (1983).

[51] A. A. Maradudin and R. F. Wallis, Phys. Rev. **123**, 777 (1961).

[52] S. N. Taraskin, S. I. Simdyankin, and S. R. Elliott, J. Phys.: Condens. Matter **19**, 455216 (2007).

[53] A. Boukenter, B. Champagnon, E. Duval, J. Dumas, J. F. Quinson, and J. Serughetti, Phys. Rev. Lett. **57**, 2391 (1986).

[54] W. Terao, T. Mori, Y. Fujii, A. Koreeda, M. Kabeya, and S. Kojima, Spectrochim. Acta A **192**, 446 (2018).

[55] J. Zhong, T. Mori, Y. Fujii, T. Kashiwagi, W. Terao, M. Yamashiro, H. Minami, M. Tsujimoto, T. Tanaka, H. Kawashima, J. Ito, M. Kijima, M. Iji, M. M. Watanabe, and K. Kadowaki, Carbohydr. Polym. **232**, 115789 (2020).

[56] T. Mori, H. Igawa, and S. Kojima, IOP Conf. Ser.: Mater. Sci. Eng. **54**, 012006 (2014).

[57] H. Igawa, T. Mori, and S. Kojima, Jpn. J. Appl. Phys. **53**, 05FE01 (2014).

[58] Y. Fujii, D. Katayama, and A. Koreeda, Jpn. J. Appl. Phys. **55**, 10TC03 (2016).

[59] H. Kawaji, T. Tojo, and T. Atake, *The 58th Calorimetry Conference, Laie, Honolulu, Hawaii*, Vol. 95 (2003), http://www.calorimetry-conference.org/CalCon2020/index.htm.

[60] J. P. Hague, J. Phys: Cond. Matt. **17**, 2397 (2005).

[61] T. Ohsaka and S. Oshikawa, Phys. Rev. B **57**, 4995 (1998).

[62] W. Hayes and R. Loudon, *Scattering of Light by Crystals* (Wiley, New York, 1978).

[63] S. N. Yannopoulos, K. S. Andrikopoulos, and G. Ruocco, J. Non-Cryst. Solids **352**, 4541 (2006).

[64] R. Shuker and R. W. Gammon, Phys. Rev. Lett. **25**, 222 (1970).

[65] N. Shimodaira, K. Saito, N. Hiramitsu, S. Matsushita, and A. J. Ikushima, Phys. Rev. B **71**, 024209 (2005).

[66] F. L. Galeener and P. N. Sen, Phys. Rev. B **17**, 1928 (1978).

[67] B. Schmid and W. Schirmacher, Phys. Rev. Lett. **100**, 137402 (2008).

[68] M. B. Enright and D. M. Leitner, Phys. Rev. E **71**, 011912 (2005).

[69] R. Burioni, D. Cassi, F. Cecconi, and A. Vulpiani, Proteins: Struct., Funct. Bioinf. **55**, 529 (2004).

[70] J. J. Grigsby, H. W. Blanch, and J. M. Prausnitz, J. Phys. Chem. B **104**, 3645 (2002).

[71] E. Duval, A. Boukenter, and T. Achibat, J. Phys.: Condens. Matter **2**, 10227 (1990).

[72] M. Fleck and A. M. Petrosyan, *Salts of Amino Acids: Crystallization, Structure and Properties* (Springer, Berlin, 2014).

[73] R. Milkus, C. Ness, V. V. Palyulin, J. Weber, A. Lapkin, and A. Zaccone, Macromolecules **51**, 1559 (2018).

[74] A. Giuntoli and D. Leporini, Phys. Rev. Lett. **121**, 185502 (2018).

[75] N. Tomoshige, H. Mizuno, T. Mori, K. Kim, and N. Matubayasi, Sci. Rep. **9**, 19514 (2019).

[76] S. G. Lushnikov, A. V. Svanidze, and I. L. Sashin, JETP Lett. **82**, 30 (2005).